

Supporting Information

S.1 Additional Results

S.1.1 Oleic acid (protonated) potentials of mean force

We measured PMFs for protonated oleic acid with the GROMOS 53a6_{OXY} and MARTINI forcefields at the water/hexadecane interface. We found the free energy to transfer oleic acid from bulk alkane to bulk water was 10 k_BT and 19 k_BT for the GROMOS 53a6_{OXY}+D and Martini forcefields, respectively. Despite this large difference in transfer free energies, the free energy differences from water to the PMF minimum were remarkably close, both -23 k_BT. The PMFs are plotted in Figure S1.

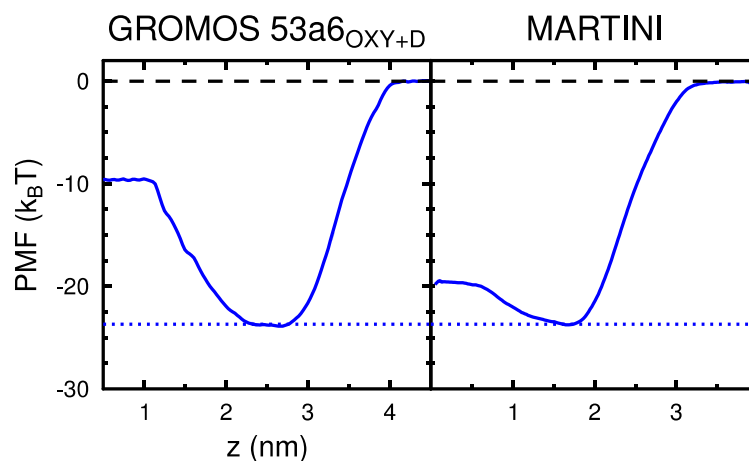


Figure S1. PMFs of oleic acid at the hexadecane/water interface in the GROMOS 53a6_{OXY}+D and MARTINI forcefields. The horizontal dotted line highlights how close the PMF minima are. PMF minima occur when the tail is removed from water into oil, with the carboxylic acid head remaining in water; z is defined so that to the left is hexadecane, to the right is water.

S.1.2 MARTINI models of hydroxyl-terminal PEG

We measured PMFs for a few oligomers using the hydroxyl-terminal modifications of the Lee et al. and Rossi et al. forcefields. We found that the trends are similar upon increasing oligomer length, and that the hydroxyl-terminal chains adsorb less strongly overall.

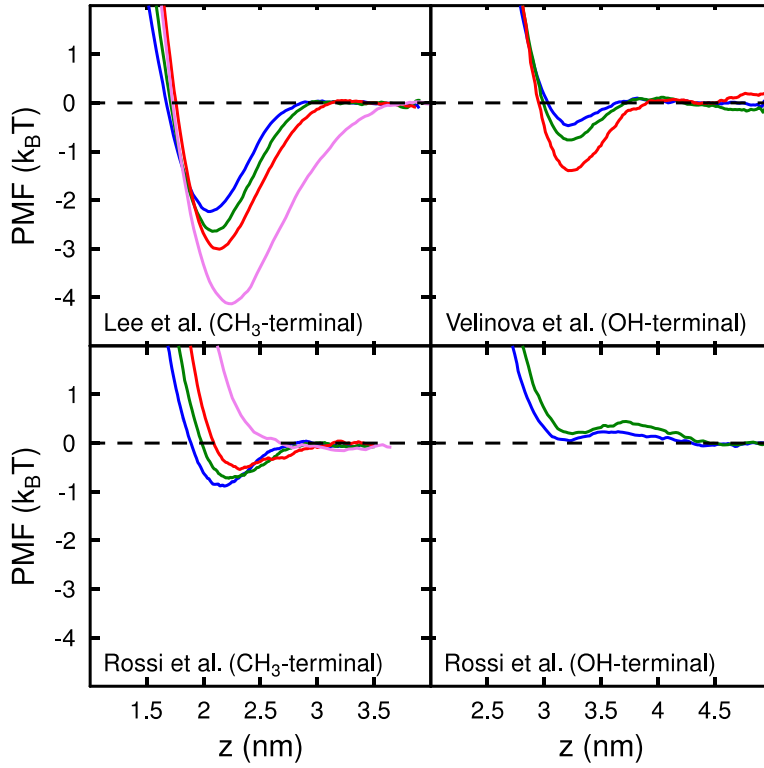


Figure S2. PMFs of methyl- and hydroxyl-terminal PEG oligomers using MARTINI forcefields by Lee et al., Velinova et al., and Rossi et al.

S.2 Derivations

S.2.1 Derivation of dilute adsorption coefficient from simulation

In this work, we assume a Tween 80 monolayer accounts for the thermodynamic surface excess of Tween 80. The Gibbs-invariant surface excess of a component $i \neq 1$ at a planar interface is given by Radke¹:

$$\Gamma_i = \Gamma_{i0} - \Gamma_{10} \left(\frac{c_i^\alpha - c_i^\beta}{c_1^\alpha - c_1^\beta} \right)$$

where Γ_i is the invariant surface excess of component i , Γ_{i0} is the surface excess of component i based on a Gibbs dividing surface at $z = z_0$, ρ_i^α is the volumetric concentration of component i in a bulk phase α .

Let bulk phase $\alpha = w$ be the aqueous phase, let bulk phase $\beta = o$ be the oil phase, let component 1 be water, and let component $i = s$ be the surfactant Tween 80 (assumed to be a single component). We can then rearrange the above equation to

$$\Gamma_s = \Gamma_{s0} - \Gamma_{10} \frac{c_s^w}{c_1^w} \left(\frac{1 - \frac{c_s^o}{c_s^w}}{1 - \frac{c_1^o}{c_1^w}} \right)$$

Because water is nearly insoluble in the oil phase, $c_1^o \ll c_1^w$. Tween 80 is also insoluble in the oil phase in the absence of reverse micelles, so $c_s^o \ll c_s^w$, and we can obtain,

$$\Gamma_s = \Gamma_{s0} \left[1 - \frac{c_s^w}{\Gamma_{s0}} \frac{\Gamma_{10}}{c_1^w} \right]$$

The adsorption coefficient of surfactant Γ_{s0}/c_s^w is safely assumed to be many orders of magnitude larger than that of water Γ_{10}/c_1^w , and so we confirm that $\Gamma_s \approx \Gamma_{s0}$. We calculate Γ_{s0} using its definition from Rowlinson and Widom.²

$$\Gamma_{s0} = \int_{-\infty}^{z_0} [c_s(z) - c_s^o] dz + \int_{z_0}^{\infty} [c_s(z) - c_s^w] dz$$

where $c_s(z)$ is the local concentration of surfactant, and c_s^o and c_s^w are the bulk concentrations of surfactant in the oil and water phases, and the division between bulk phases is set by a Gibbs dividing surface at $z = z_0$.

We divide by c_s^w to obtain an adsorption coefficient

$$\frac{\Gamma_{s0}}{c_s^w} = \int_{-\infty}^{z_0} \left[\frac{c_s(z)}{c_s^w} - \frac{c_s^o}{c_s^w} \right] dz + \int_{z_0}^{\infty} \frac{c_s(z)}{c_s^w} - 1 dz$$

For a surfactant interfacial potential of mean force (PMF) W_z shifted so that $W_z = 0$ in the bulk water, we have by the Boltzmann equation

$$\frac{\Gamma_{s0}}{c_s^w} = \int_{-\infty}^{z_0} \left[e^{-\beta W_z(z)} - \frac{c_s^o}{c_s^w} \right] dz + \int_{z_0}^{\infty} [e^{-\beta W_z(z)} - 1] dz \quad (\text{S1})$$

From this formula, we can obtain the adsorption coefficient Γ_{s0}/c_s^w from an PMF, assuming the simulation accurately models equilibrium conditions. We seek the dilute-limit ‘‘Henry’s law’’ adsorption coefficient for which surfactant molecules do not interact with each other, so a lone Tween 80 molecule at a clean water-oil interface is the correct environment to simulate.

In practice, we do not numerically evaluate the integral from $-\infty$ to $+\infty$. We evaluate over a finite range which encompasses the interface and the contribution from $e^{-\beta W_z(z)}$ around the PMF minimum. Since the magnitude of $c_s(z)$ at the interface is many orders greater than c_s^w and c_s^o , positioning of the Gibbs dividing surface z_0 is not needed.

S.2.2 Derivation of dilute adsorption coefficient from Nikas-Mulqueen-Blankschtein (NMB) Theory

In this work, we refer to the ‘‘adsorption free energy’’ parameter in Nikas-Mulqueen-Blankschtein theory as the *dilute adsorption free energy*. We derive Equation 5 from the manuscript below and verify that the *dilute adsorption free energies* $\Delta\mu_i^0$ from Nikas, Puvvada,

and Blankschtein³ and $\Delta\mu_i^{\sigma/w,0}$ from Mulqueen and Blankschtein⁴ have the same relation to the dilute adsorption coefficient, save for a dependence on the units of the adsorption coefficient.

Starting from Equation 5 in Nikas et al.,³

$$\mu_i^\sigma = \mu_i^{\sigma,0} + k_B T \left[\ln \frac{x_i^\sigma}{a - \sum_j x_j^\sigma a_j} + \frac{a_i + 2\pi r_i \sum_j x_j^\sigma r_j}{a - \sum_j x_j^\sigma a_j} + \frac{\pi a_i (\sum_j x_j^\sigma r_j)^2}{(a - \sum_j x_j^\sigma a_j)^2} \right] + \frac{2}{a} \sum_j B_{ij} x_j^\sigma$$

a is the total area available per adsorbed surfactant molecule, i.e. $\frac{A}{N}$ where A is the total area and N is the total number of surfactant molecules adsorbed to the interface.

a_i is the hard disk area of a surfactant species i based on its hard disk radius r_i

x_i^σ is the mole fraction of surfactant i at the interface, i.e. N_i/N

Firstly, we make simplifications to consider only a single surfactant species. E.g. $x_j^\sigma = 1$ and we rewrite the radii r_i in terms of areas a_i .

$$\mu_i^\sigma = \mu_i^{\sigma,0} + k_B T \left[\ln \frac{1}{a - a_i} + \frac{3a_i}{a - a_i} + \frac{a_i^2}{(a - a_i)^2} \right] + \frac{2}{a} B_{ii}$$

Secondly, we take the dilute limit, such that $a \gg a_i$ and $a \gg B_{ii}$.

$$\mu_i^\sigma = \mu_i^{\sigma,0} + k_B T \ln \frac{1}{a}$$

Thirdly, we recognize that $1/a$ is the quantity N/A which we write as Γ .

$$\mu_i^\sigma = \mu_i^{\sigma,0} + k_B T \ln \Gamma$$

Although the precise definition of Γ with respect to a Gibbs dividing surface or some other thermodynamic formalism

I leave this result for now and turn to the chemical potential write in terms of bulk phase properties. Starting from Equation 6 in Nikas et al.,

$$\mu_A^b = \mu_A^{b,0} + k_B T \left[\ln X_{1A} + X - \sum_{n_A, n_B} X_{n_A, n_B} \right]$$

X_{1A} is the bulk mole fraction of surfactant monomer type A.

X is the bulk mole fraction of surfactant.

X_{n_A, n_B} are the bulk mole fraction of mixed micelles.

Consider only a single surfactant species in the dilute limit well below the critical micelle concentration,

$$\mu_A^b = \mu_A^{b,0} + k_B T [\ln X + X]$$

In the dilute limit, $\lim_{X \rightarrow 0} X = 0$ but $\lim_{X \rightarrow 0} \ln X$ will remain important.

$$\mu_A^b = \mu_A^{b,0} + k_B T \ln X$$

The chemical potentials μ_A^σ and μ_A^b are equal at equilibrium. Setting them equal, we obtain an equation governing equilibrium for a single surfactant in the dilute limit:

$$\mu_A^{\sigma,0} - \mu_A^{b,0} = -k_B T \ln \frac{\Gamma}{X}$$

$$\Delta\mu_i^0 = -k_B T \ln \frac{\Gamma}{X}$$

where Γ is the dimensional surface density and X is the bulk phase mole fraction of surfactant. Furthermore, we can write,

$$\frac{\Gamma}{c_s^w} = c_w^w e^{-\Delta\mu_i^0/k_B T} \quad (\text{S2})$$

where c_s^w is the concentration of surfactant molecules in bulk water, and c_w^w is the concentration of water in bulk water. This is valid in the dilute limit because $c_s^w \ll c_w^w$ so $\frac{c_s^w}{c_w^w} \approx X$.

Equation 5 in Mulqueen and Blankshtein can be transformed to Equation 5 in Nikas et al. with a simple transformation: divide numerator and denominator by Γ as needed.

$$\mu_i^\sigma = \mu_i^{\sigma,0} + k_B T \left[\ln \left(\frac{\Gamma_i}{1 - \sum_{k=1}^n \Gamma_k a_k} \right) + \frac{a_i + 2\pi r_i \sum_{k=1}^n \Gamma_k r_k}{1 - \sum_{k=1}^n \Gamma_k a_k} + \frac{\pi a_i (\sum_{k=1}^n \Gamma_k r_k)^2}{(1 - \sum_{k=1}^n \Gamma_k a_k)^2} \right]$$

Actually, this doesn't quite get you the same result. There appears to be a typo in the second term in square brackets, and the above should be:

$$\mu_i^\sigma = \mu_i^{\sigma,0} + k_B T \left[\ln \left(\frac{\Gamma_i}{1 - \sum_{k=1}^n \Gamma_k a_k} \right) + \frac{\Gamma a_i + 2\pi r_i \sum_{k=1}^n \Gamma_k r_k}{1 - \sum_{k=1}^n \Gamma_k a_k} + \frac{\pi a_i (\sum_{k=1}^n \Gamma_k r_k)^2}{(1 - \sum_{k=1}^n \Gamma_k a_k)^2} \right]$$

Equation 6 from Mulqueen and Blankshtein gives the chemical potential for a surfactant molecule in the aqueous phase:

$$\mu_i^w = \mu_i^{w,0} + k_B T \ln \left(\frac{n_i^w}{n_w^w} \right)$$

where n_i^w is the concentration of surfactant molecules of type i in the aqueous phase and n_w^w is the concentration of water molecules in the aqueous phase. For a single species, n_i^w

Because Equation 5 from Mulqueen and Blankschtein can be transformed to Equation 5 from Nikas et al., it can also be simplified in the dilute limit to Equation S2. Setting the chemical potentials equal,

$$\mu_i^{\sigma,0} - \mu_i^{w,0} = -k_B T \ln \frac{n_w^w \Gamma}{n_i^w}$$

Again, we can write

$$\frac{\Gamma}{n_i^w} = n_w^w e^{-\Delta\mu_i^{\sigma/w,0}/k_B T} \quad (\text{S3})$$

and observe by comparison of Equations S2 and S3 that $\Delta\mu_i^0$ and $\Delta\mu_i^{\sigma/w,0}$ from the two papers are functionally equivalent.

Note there is a difference between these adsorption free energies and the value used in the body of this paper. For Mulqueen and Blankschtein, $\Delta\mu_i^{\sigma/w,0} = \mu_i^{\sigma,0} - \mu_i^{w,0}$. We defined it instead $\Delta\mu_i^{\sigma/w,0} = \mu_i^{\sigma,0} - \mu_i^{w,0} + k_B T \ln c_w^w$ which gives $\Delta\mu_i^{\sigma/w,0}$ the simpler relation to the adsorption coefficient, shown in Equations 6, 7, and 9. Comparison with Equation S1 shows that the dilute adsorption free energy can be calculated from the PMF of an isolated surfactant.

S.2.3 Derivation of marginal excess pressure-area work integral in terms of intensive area a

Starting from Equation 4 in Nikas et al.,³ we make a substitution $\mu_s^{\sigma,0} = \tilde{\mu}_i^{\sigma,0} + k_B T \left(1 + \ln \left(\frac{k_B T}{\Pi_0}\right)\right)$ and $\Pi^{\text{id}} = \Gamma_s k_B T$ and observe that $x_i^\sigma = 1$ for a single component to obtain:

$$\mu_s^\sigma = \mu_s^{\sigma,0} + \ln \Gamma_s - \int_{\infty}^A \left(\frac{\partial \left(\Pi(A', N_s^\sigma) - \Pi^{\text{id}}(A', N_s^\sigma) \right)}{\partial N_s^\sigma} \right)_{A', T, p} dA'$$

Surface pressure $\Pi(A, N_s^\sigma)$ is a function of the intensive area per molecule $\Pi(A, N_s^\sigma) = \Pi(a)$ where $a = \frac{A}{N_s^\sigma}$. We note that the integral above comes from the expression below:

$$\frac{\partial}{\partial N_s^\sigma} \left[\int_{\infty}^A \left(\Pi(A', N_s^\sigma) - \Pi^{\text{id}}(A', N_s^\sigma) \right) dA' \right]_{A, p, T}$$

The Π - A integral follows a path of constant N_s^σ , and the partial derivative $\frac{\partial}{\partial N_s^\sigma} |_{A, p, T}$ measures the marginal change in that integral upon adding an adsorbed surfactant without changing the area.

$$\int_{\infty}^A \left(\frac{\partial \left(\Pi(A', N_s^\sigma) - \Pi^{\text{id}}(A', N_s^\sigma) \right)}{\partial N_s^\sigma} \right)_{A', T, p} dA'$$

Our task is simply to transform this expression from extensive coordinates $\{N_s^\sigma, A\}$ to the intensive area a . We will use the differential:

$$A = N_s^\sigma a$$

$$dA = N_s^\sigma da + dN_s^\sigma a$$

The partial derivative is taken along $dA = 0$, so we can use a simple chain rule to transform it:

$$0 = N_s^\sigma da + dN_s^\sigma a$$

$$\frac{\partial a}{\partial N_s^\sigma} = -\frac{a}{N_s^\sigma}$$

$$\begin{aligned} & \left(\frac{\partial \left(\Pi(A', N_s^\sigma) - \Pi^{\text{id}}(A', N_s^\sigma) \right)}{\partial N_s^\sigma} \right)_{A', T, p} \\ &= \left(\frac{\partial \left(\Pi(A', N_s^\sigma) - \Pi^{\text{id}}(A', N_s^\sigma) \right)}{\partial a'} \right)_{A', T, p} \left(\frac{\partial a'}{\partial N_s^\sigma} \right)_{A', T, p} \\ &= - \left(\frac{\partial \left(\Pi(A', N_s^\sigma) - \Pi^{\text{id}}(A', N_s^\sigma) \right)}{\partial a'} \right)_{A', T, p} \frac{a'}{N_s^\sigma} \end{aligned}$$

Over the integration, we have $dN_s^\sigma = 0$, so the differential area $dA' = N_s^\sigma da'$. When we change the variable of integration, we also change the bounds of integration:

$$A' = \infty \rightarrow a' = \infty$$

$$A' = A \rightarrow a' = a$$

$$\int_{\infty}^A \dots dA' \rightarrow \int_{\infty}^a \dots da'$$

Putting this together, we obtain

$$\begin{aligned} & - \int_{\infty}^a \left(\frac{\partial \left(\Pi(A', N_s^\sigma) - \Pi^{\text{id}}(A', N_s^\sigma) \right)}{\partial a'} \right)_{A', T, p} \frac{a'}{N_s^\sigma} N_s^\sigma da' \\ & - \int_{\infty}^a \left(\frac{\partial \left(\Pi(A', N_s^\sigma) - \Pi^{\text{id}}(A', N_s^\sigma) \right)}{\partial a'} \right)_{A', T, p} a' da' \end{aligned}$$

Yielding our final expression of the surface chemical potential equation in terms of intensive area.

$$\mu_s^\sigma = \mu_s^{\sigma,0} + \ln \Gamma_s + \int_{\infty}^a \left(\frac{\partial (\Pi(a') - \Pi^{\text{id}}(a'))}{\partial a'} \right)_{A',T,p} a' da'$$

S.3 Analysis Method Details

S.3.1 Dilute Adsorption Free Energy from Simulation and its Uncertainty

Given the PMF $W_Z(z)$ for an isolated surfactant at a clean water/oil interface, we can calculate the dilute adsorption free energy by comparing Equations 6 and 10.

$$\Delta\mu^{\sigma/w,0} = -k_B T \ln \left[\int_{-\infty}^{z_0} \left[e^{-\beta W_Z(z)} - \frac{c_s^0}{c_s^w} \right] dz + \int_{z_0}^{\infty} [e^{-\beta W_Z(z)} - 1] dz \right]$$

To obtain the uncertainty in adsorption free energies calculated from PMFs using this equation, we generated 1,000 bootstrapped PMFs with *g_wham*. These bootstrapped PMFs were vertically shifted such that the average W_Z in the horizontal section was equal to zero. Dilute adsorption free energy $\Delta\mu^{\sigma/w,0}$ was calculated from each vertically-shifted, bootstrapped PMF. Subtracting 1,000 bootstrapped $\Delta\mu^{\sigma/w,0}$ for C₁₂E₂ from each of the 1,000 bootstrapped $\Delta\mu^{\sigma/w,0}$ for C₁₂E₈, we obtained 1,000,000 $\Delta\Delta\mu^{\sigma/w,0}$ for the difference between C₁₂E₂ and C₁₂E₈. From this distribution of $\Delta\Delta\mu^{\sigma/w,0}$, we calculated the 2.5 and 97.5 percentiles to determine the 95% confidence interval.

For GROMOS 53a6_{OXY+D}, the lower and upper limits of the 95% confidence interval were 6.77 and 8.14, with a mean of 7.47, so we reported $\Delta\Delta\mu^{\sigma/w,0} = 7.5 \pm 0.7$ k_BT.

For MARTINI (Lee et al.), the lower and upper limits of the 95% confidence interval were 1.33 and 1.85, with a mean of 1.58, so we reported $\Delta\Delta\mu^{\sigma/w,0} = 1.6 \pm 0.3$ k_BT.

S.3.2 Marginal Excess Pressure-Area Work

The pressure-area isotherm is interpolated from pressure-area data using a piecewise function with a sum of exponentials and a 2D vdW-like excluded-area equation of state:

$$\Pi = \begin{cases} p_0 + \sum_{i=1}^n p_i e^{-q_i(a-a_0)} & \text{for } a < a_{\text{switch}} \\ \frac{k_B T}{a - A} & \text{for } a > a_{\text{switch}} \end{cases} \quad (\text{S4})$$

We write the marginal excess pressure-area work (MEPAW) integral

$$\int_{\infty}^a \frac{\partial (\Pi(a') - \Pi_{\text{id}}(a'))}{\partial a'} a' da'$$

and substitute the piecewise functional form of the $\Pi(a)$ isotherm.

$$\int_{a_{\text{switch}}}^a \frac{\partial}{\partial a'} (\Pi_{\text{SoE}}(a'; \{p_i\}, \{q_i\}, a_0) - \Pi_{\text{id}}(a')) a' da' + \int_{\infty}^{a_{\text{switch}}} \frac{\partial}{\partial a'} (\Pi_{\text{vdW}}(a'; A) - \Pi_{\text{id}}(a')) a' da'$$

We evaluate the sum of exponentials piece:

$$\int_{a_{\text{switch}}}^a \frac{\partial (\Pi_{\text{SoE}}(a'; \{p_i\}, \{q_i\}, a_0) - \Pi_{\text{id}}(a'))}{\partial a'} a' da'$$

$$\int_{a_{\text{switch}}}^{a_2} \frac{\partial (p_0 + \sum_{i=1}^n p_i e^{-q_i(a'-a_0)} - k_B T/a')}{\partial a'} a' da'$$

$$\int_{a_{\text{switch}}}^{a_2} \frac{\partial (\sum_{i=1}^n p_i e^{-q_i(a'-a_0)} - k_B T/a')}{\partial a'} a' da'$$

$$\int_{a_{\text{switch}}}^{a_2} \left(-\sum_{i=1}^n p_i q_i e^{-q_i(a'-a_0)} + \frac{k_B T}{a'^2} \right) a' da'$$

$$\int_{a_{\text{switch}}}^{a_2} -\sum_{i=1}^n p_i q_i e^{-q_i(a'-a_0)} a' + \frac{k_B T}{a'} da'$$

$$\int_{a_{\text{switch}}}^{a_2} -\sum_{i=1}^n p_i q_i e^{-q_i(a'-a_0)} a' + \frac{k_B T}{a'} da'$$

$$\left[\sum_{i=1}^n \frac{p_i q_i e^{-q_i(a'-a_0)} (q_i a' + 1)}{q_i^2} + k_B T \log a' \right]_{a_{\text{switch}}}^{a_2}$$

$$\sum_{i=1}^n \frac{p_i}{q_i} \left(e^{-q_i(a-a_0)} (q_i a + 1) - e^{-q_i a_{\text{switch}} - a_0} (q_i a_{\text{switch}} + 1) \right) + k_B T \log \frac{a}{a_{\text{switch}}}$$

And the 2D vdW piece:

$$\int_{\infty}^{a_{\text{switch}}} \frac{\partial}{\partial a'} \left(-\frac{k_B T}{A - a'} - \frac{k_B T}{a'} \right) a' da'$$

$$\int_{\infty}^{a_{\text{switch}}} \frac{\partial}{\partial a'} \left(-\frac{k_B T}{A - a'} - \frac{k_B T}{a'} \right) a' da'$$

$$k_B T \left[\frac{A}{a_{\text{switch}} - A} + \log \left(\frac{a_{\text{switch}}}{a_{\text{switch}} - A} \right) \right]$$

Adding these two pieces, we obtain the MEPAW at a given area per molecule a . Note that if $a \leq a_{\text{switch}}$, only the 2D vdW piece needs to be evaluated.

In fitting the parameters, a_{switch} is simply set to the maximum a in the pressure-area data set, a_0 is set to the minimum a in the pressure-area data set, and $\{p_i\}, \{q_i\}$ are fitted using the Kaufmann (2003) scheme, implemented at <https://github.com/khuston/Kaufmann2003>. This scheme will fit the data with $1 + 2n$ parameters (p_0 and p_i, q_i for $i \in [1, n]$). The script used as large an n as possible, so long as parameters p_i and q_i were positive. [For GROMOS 53a6_{OXY+D} Tween 80, the fitting parameters were \$p_0 = 0.2323, p_1 = 38.5993, q_1 = 0.4657\$. In almost all cases, this resulted in \$n = 2\$, or 5 parameters for a two-exponential fit.](#)

S.3.2 Intramolecular density contour plots

To make the intramolecular density contour plots, a sample of atomic coordinates from the last 20 ns of monolayer simulation was converted from Cartesian (x, y, z) to cylindrical (r, z) coordinates, where the direction z points along the interface normal from oil into water. The coordinate system is defined relative to a central atom (chosen to be the ester carbon, in this case) and the vector $(0, 0, 1)$. Atomic positions are binned into a 2D histogram on r, z . Note that bins at larger r collect points from a larger cylindrical shell, whose volume scales as r . For this reason, the density was normalized with respect to this increasing shell volume. The plots are meant to be qualitative, so the atoms were weighted equally in binning. The contour values were at a fixed number density of atoms in the group (either head or tail).

S.3.4 Note on Hysteresis

Hysteresis arises from inadequate sampling of the simulated system. Molecular dynamics simulation samples configuration space by following Newton's equations of motion, which provide the correct Boltzmann weighting if ergodicity is given, but MD is inefficient at crossing high-energy barriers. Such an energy barrier exists between "tail-extended" and "tail-retracted" states (see Fig. S3):

- In outward pulling, the tail begins in contact with the oil. As Tween 80 pulls away, the tail lingers in contact, so the "tail-extended" state is initially sampled. If this "tail-extended" state is overrepresented, the calculated PMF will be artificially deep.
- In inward pulling, the tail begins in aqueous solution. As Tween 80 approaches, the tail eventually extends to contact the interface, but the "tail-retracted" state is initially over-

sampled, and if the inward pulling is not extremely slow, this overrepresentation is not averaged out and the calculated PMF will be artificially shallow.

For the oleate tail to pass between “tail-extended” and “tail-retracted” states, it must break contact with the oil and then retract. This process has a free energy barrier that makes passage between the two states difficult. Given sufficient time to sample, the PMFs calculated from inward and outward pulling will converge to the correct PMF. Otherwise, the calculated PMFs will bracket the correct PMF. In the PMF generated by inward pulling (solid line in Figure S3), sharp jumps (e.g. point “B” in Figure S3) near the profile’s right end are due to simulation windows in which the tail contacted and stuck to the oil. Some adjacent windows did not have enough time for the oleate tail to contact the interface; the Tween 80 feels an isotropic environment, and the PMF remains horizontal (e.g. points “C” in Figure S3).

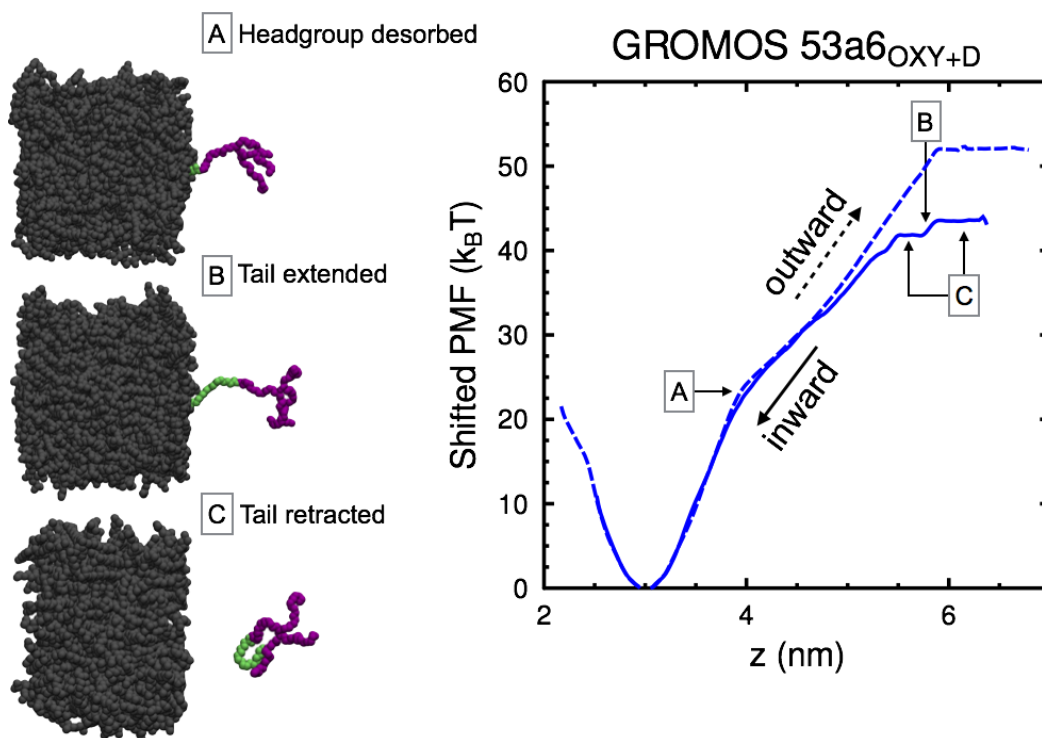


Figure S3. Above, non-converged PMFs of Tween 80 at the clean water/squalane interface are zeroed at their minima to highlight their overlap near the interface and divergence toward aqueous bulk. “A” separates tail desorption (to its right) from headgroup desorption (to its left). “B” and “C” point to sections of the inward-pulling PMF that are based on tail-extended and tail-retracted windows, respectively. The tail-extended windows cause abrupt jumps in the PMF. These are separated by horizontal stretches where the surfactant with retracted tail senses an isotropic environment.

Advanced sampling techniques may hop the barrier between extended and retracted states more quickly, yielding the correct PMF without brute-force MD simulation. For this study, we contented ourselves with bracketing the correct profiles in some cases where even with the

uncertainty in the exact depth of the potential, we could still make strong conclusions about the irreversibility of the adsorption.

S.3.4 2D-biased umbrella sampling to obtain 1D PMF

We introduced a second harmonic bias on the surfactant tail's center of mass Y (Fig. S4). With the resulting 2D-biased trajectories, we used Grossfield's WHAM⁵ to output the 2D potential of mean force W_{ZY} :

$$W_{ZY}(z, y) = -k_B T \ln \rho_{ZY}(z, y) + C \quad (\text{S5})$$

where ρ_{ZY} is the unbiased joint probability density of finding the molecule at $Z = z$ and $Y = y$, k_B is Boltzmann's constant, T is the simulation temperature (300 K), and C is an arbitrary PMF shift independent of z and y . We could then integrate the joint probability ρ_{ZY} along Y to obtain the 1D PMF.

$$W_Z(z) = -k_B T \ln \left[\int e^{-\frac{W_{ZY}(z,y)}{k_B T}} dy \right] + B \quad (\text{S6})$$

Following the convention in Equation 1, the constant B shifts W_Z vertically to be zero in bulk water.

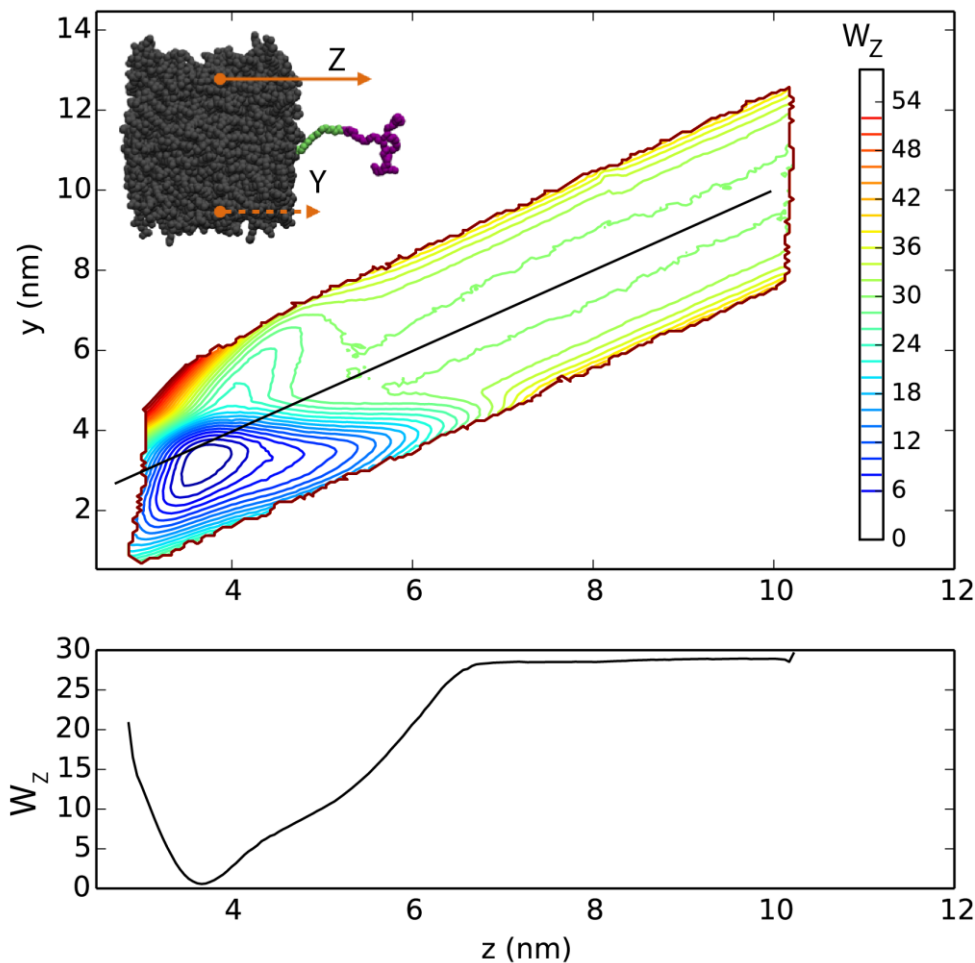


Figure S4. The upper plot shows colored contours of constant PMF W_{ZY} sampled for Tween 80 using the MARTINI (Lee et al.) forcefield. The line $y = z$ is superimposed on the contour plot in black. Following this line to large z , we see W_{ZY} becomes symmetric in y where the surfactant no longer makes contact with the interface, as expected. The lower plot shows the 1D PMF W_Z that results from integrating over tail positions y (Eqn. S6). The two reduced coordinates Z (surfactant center of mass) and Y (tail center of mass) are illustrated in the inlaid image.

To generate initial configurations for 2D-biased sampling, we restrained the surfactant center of mass at a series of positions along Z , and for each z , we pulled the tail center of mass to a series of positions along Y . This provided a grid of initial configurations in (Z, Y) space to launch simulations for the 2D PMF plotted with contours in the upper part of Figure S4. Harmonic spring constants for Z and Y were 1000 and $250 \text{ kJ mol}^{-1} \text{ nm}^{-2}$, respectively.

S.3.5 Partial sampling of 2D PMF

Contributions to the adsorption coefficient drop off exponentially with increases in the PMF (see Equation 8). When the tail is pulled far enough, i.e. when y deviates far enough from the $z = y$ line, the PMF increases monotonically with increasing distance. Thus, coordinate space beyond this point with PMF more than several $k_B T$ greater than the PMF minimum can be neglected.

Hysteretic sections of the 1D PMF could be avoided altogether by carving a path through the 2D (z,y) space to bridge two regions which adequately sample y . We used such a scheme in generating the 1D PMFs for the Rossi et al. Tween 80. Figure S5 highlights in gray the section around 7-11 nm in which y was not fully sampled, and a narrow path was taken from the adsorption basin to the bulk. The section of W_Z highlighted in gray is then not in fact a PMF, but an artifact of the integrating the partially-sampled 2D space.

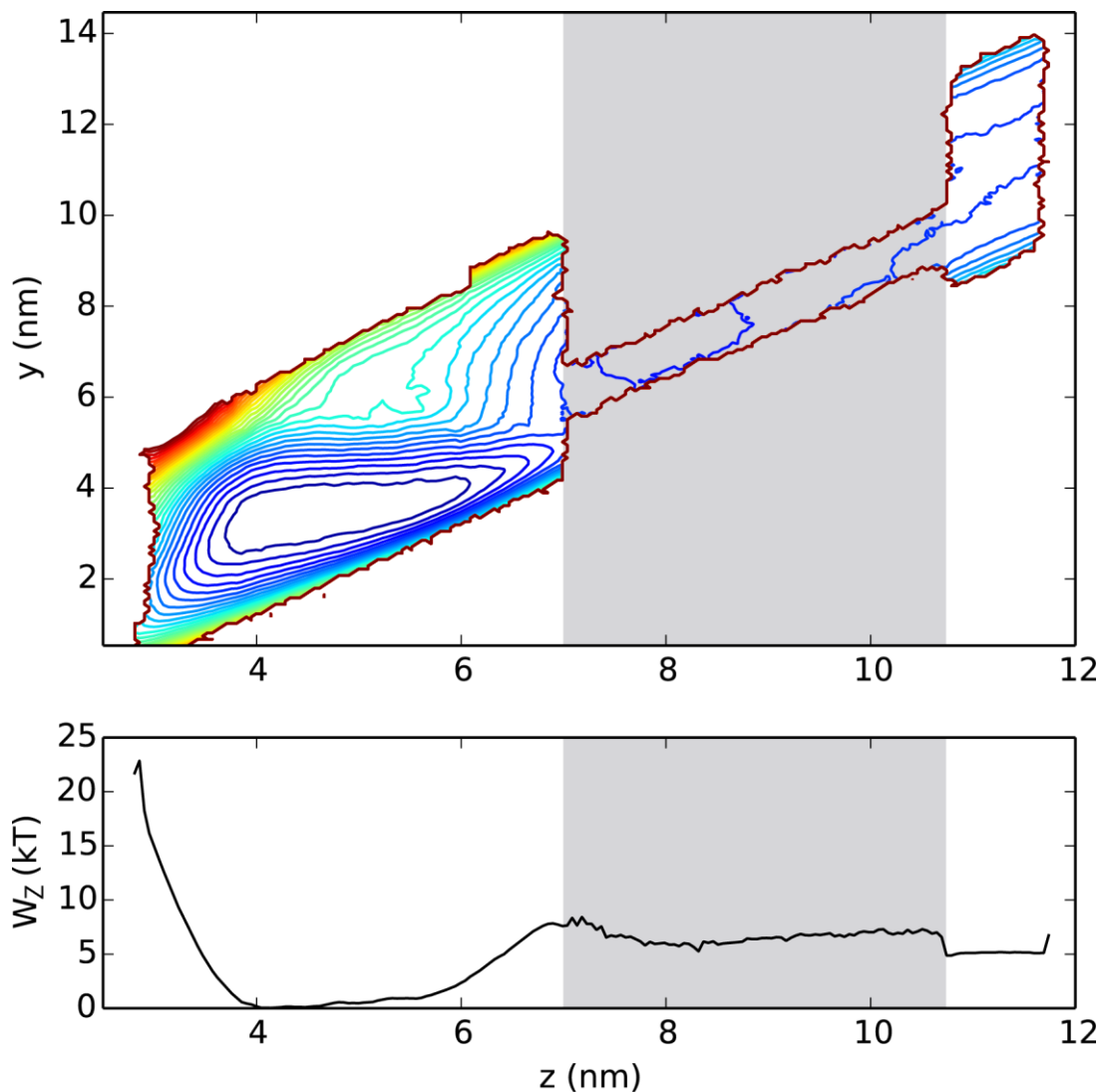


Figure S5. The plots are grayed where the sampled 2D space is missing significant contributions to the partition function at a given z . Thus the integrated 1D PMF is meaningless in that region. However, a path is established in 2D space between the adsorbed region (left) and bulk region (right), and differences in the 1D PMF between these regions are accurate, so long as the PMF difference along the 2D path is accurate.

S.4 Molecular Simulation Details

S.4.1 SMILES Strings

PEG3 (hydroxyl-terminal)

OCCOCCOCCO

PEG5 (hydroxyl-terminal)

OCCOCCOCCOCCOCCO

PEG8 (hydroxyl-terminal)

OCCOCCOCCOCCOCCOCCOCCOCCO

PEO3 (methyl-terminal)

COCCOCCOC

PEO5 (methyl-terminal)

COCCOCCOCCOCCOC

PEO8 (methyl-terminal)

COCCOCCOCCOCCOCCOCCOCCOC

S.4.2 Coarse-grained structure schematics

PEO3, Lee et al. (methyl-terminal)



PEO5, Lee et al. (methyl-terminal)



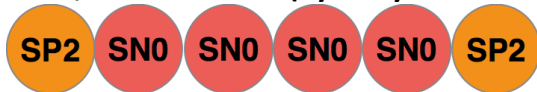
PEO8, Lee et al. (methyl-terminal)



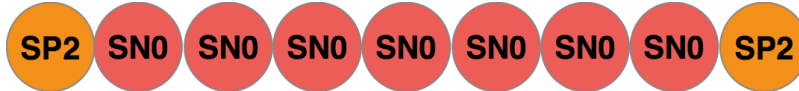
PEG3, Velinova et al. (hydroxyl-terminal)



PEG5, Velinova et al. (hydroxyl-terminal)



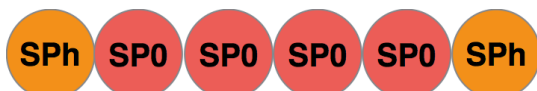
PEG8, Velinova et al. (hydroxyl-terminal)



PEG3, Rossi et al. (hydroxyl-terminal)



PEG5, Rossi et al. (hydroxyl-terminal)



PEG8, Rossi et al. (hydroxyl-terminal)



S.4.3 Gromacs Included Topology (.itp) files

Some .itp files are printed here for reference.

PEO3 – Martini, Lee et al. (-CH₃ terminal)

```
#define peob 1 0.33 17000.0
#define peoa 1 130.0 50.0
#define peod1 1 180.0 1.96 1.0
#define peod3 1 0.0 0.33 3.0
#define peod2 1 0.0 0.18 2.0
#define peod4 1 0.0 0.12 4.0

[ moleculetype ]
; Name nrexcl
LIG 1

[ atoms ]
; nr type resnr resname atom cgnr charge mass ;
 1 SN0 1 LIG A1 1 0 54 ;
 2 SN0 1 LIG A2 2 0 54 ;
 3 SN0 1 LIG A3 3 0 54 ;

[ bonds ]
; ai aj fu c0, c1, ...
 1 2 peob ;
 2 3 peob ;

[ angles ]
; ai aj ak fu c0, c1, ...
 1 2 3 peoa ;
```

PEO5 – Martini, Lee et al. (-CH₃ terminal)

```
#define peob 1 0.33 17000.0
#define peoa 1 130.0 50.0
#define peod1 1 180.0 1.96 1.0
#define peod3 1 0.0 0.33 3.0
#define peod2 1 0.0 0.18 2.0
#define peod4 1 0.0 0.12 4.0

[ moleculetype ]
; Name nrexcl
LIG 1

[ atoms ]
; nr type resnr resname atom cgnr charge mass ;
1 SN0 1 LIG A1 1 0 54 ;
2 SN0 1 LIG A2 2 0 54 ;
3 SN0 1 LIG A3 3 0 54 ;
4 SN0 1 LIG A4 4 0 54 ;
5 SN0 1 LIG A5 5 0 54 ;

[ bonds ]
; ai aj fu c0, c1, ...
1 2 peob ;
2 3 peob ;
3 4 peob ;
4 5 peob ;

[ angles ]
; ai aj ak fu c0, c1, ...
1 2 3 peoa ;
2 3 4 peoa ;
3 4 5 peoa ;

[ dihedrals ]
; ai aj ak al fu c0, c1, ...
1 2 3 4 peod1 ;
1 2 3 4 peod3 ;
1 2 3 4 peod2 ;
1 2 3 4 peod4 ;
2 3 4 5 peod1 ;
2 3 4 5 peod3 ;
2 3 4 5 peod2 ;
2 3 4 5 peod4 ;
```

PEO8 – Martini, Lee et al. (-CH₃ terminal)

```

#define peob 1 0.33 17000.0
#define peoa 1 130.0 50.0
#define peod1 1 180.0 1.96 1.0
#define peod3 1 0.0 0.33 3.0
#define peod2 1 0.0 0.18 2.0
#define peod4 1 0.0 0.12 4.0

[ moleculetype ]
; Name nrexcl
LIG 1

[ atoms ]
; nr type resnr resname atom cgnr charge mass
1 SNO 1 LIG A1 1 0 54 ;
2 SNO 1 LIG A2 2 0 54 ;
3 SNO 1 LIG A3 3 0 54 ;
4 SNO 1 LIG A4 4 0 54 ;
5 SNO 1 LIG A5 5 0 54 ;
6 SNO 1 LIG A6 6 0 54 ;
7 SNO 1 LIG A7 7 0 54 ;
8 SNO 1 LIG A8 8 0 54 ;

[ bonds ]
; ai aj fu c0, c1, ...
1 2 peob ;
2 3 peob ;
3 4 peob ;
4 5 peob ;
5 6 peob ;
6 7 peob ;
7 8 peob ;

[ angles ]
; ai aj ak fu c0, c1, ...
1 2 3 peoa ;
2 3 4 peoa ;
3 4 5 peoa ;
4 5 6 peoa ;
5 6 7 peoa ;
6 7 8 peoa ;

[ dihedrals ]
; ai aj ak al fu c0, c1, ...
1 2 3 4 peod1 ;
1 2 3 4 peod3 ;
1 2 3 4 peod2 ;
1 2 3 4 peod4 ;
2 3 4 5 peod1 ;
2 3 4 5 peod3 ;
2 3 4 5 peod2 ;
2 3 4 5 peod4 ;
3 4 5 6 peod1 ;
3 4 5 6 peod3 ;
3 4 5 6 peod2 ;
3 4 5 6 peod4 ;
4 5 6 7 peod1 ;
4 5 6 7 peod3 ;
4 5 6 7 peod2 ;
4 5 6 7 peod4 ;
5 6 7 8 peod1 ;
5 6 7 8 peod3 ;
5 6 7 8 peod2 ;
5 6 7 8 peod4 ;

```


PEG3 – Martini, Velinova et al. (-OH terminal)

```
#define peob 1 0.33 17000.0
#define peoa 1 130.0 50.0
#define peod1 1 180.0 1.96 1.0
#define peod3 1 0.0 0.33 3.0
#define peod2 1 0.0 0.18 2.0
#define peod4 1 0.0 0.12 4.0

[ moleculetype ]
; Name nrexcl
LIG 1

[ atoms ]
; nr type resnr resname atom cgnr charge mass
1 SP2 1 LIG A1 1 0 54 ;
2 SN0 1 LIG A2 2 0 54 ;
3 SN0 1 LIG A3 3 0 54 ;
4 SP2 1 LIG A4 4 0 54 ;

[ bonds ]
; ai aj fu c0, c1, ...
1 2 peob ;
2 3 peob ;
3 4 peob ;

[ angles ]
; ai aj ak fu c0, c1, ...
1 2 3 peoa ;
2 3 4 peoa ;

[ dihedrals ]
; ai aj ak al fu c0, c1, ...
1 2 3 4 peod1 ;
1 2 3 4 peod3 ;
1 2 3 4 peod2 ;
1 2 3 4 peod4 ;
```

PEG5 – Martini, Velinova et al. (-OH terminal)

```
#define peob 1 0.33 17000.0
#define peoa 1 130.0 50.0
#define peod1 1 180.0 1.96 1.0
#define peod3 1 0.0 0.33 3.0
#define peod2 1 0.0 0.18 2.0
#define peod4 1 0.0 0.12 4.0

[ moleculetype ]
; Name nrexcl
LIG 1

[ atoms ]
; nr type resnr resname atom cgnr charge mass ;
1 SP2 1 LIG A1 1 0 54 ;
2 SN0 1 LIG A2 2 0 54 ;
3 SN0 1 LIG A3 3 0 54 ;
4 SN0 1 LIG A4 4 0 54 ;
5 SN0 1 LIG A5 5 0 54 ;
6 SP2 1 LIG A6 6 0 54 ;

[ bonds ]
; ai aj fu c0, c1, ...
1 2 peob ;
2 3 peob ;
3 4 peob ;
4 5 peob ;
5 6 peob ;

[ angles ]
; ai aj ak fu c0, c1, ...
1 2 3 peoa ;
2 3 4 peoa ;
3 4 5 peoa ;
4 5 6 peoa ;

[ dihedrals ]
; ai aj ak al fu c0, c1, ...
1 2 3 4 peod1 ;
1 2 3 4 peod3 ;
1 2 3 4 peod2 ;
1 2 3 4 peod4 ;
2 3 4 5 peod1 ;
2 3 4 5 peod3 ;
2 3 4 5 peod2 ;
2 3 4 5 peod4 ;
3 4 5 6 peod1 ;
3 4 5 6 peod3 ;
3 4 5 6 peod2 ;
3 4 5 6 peod4 ;
```

PEG8 – Martini, Velinova et al. (-OH terminal)

```
#define peob 1 0.33 17000.0
#define peoa 1 130.0 50.0
#define peod1 1 180.0 1.96 1.0
#define peod3 1 0.0 0.33 3.0
#define peod2 1 0.0 0.18 2.0
#define peod4 1 0.0 0.12 4.0

[ moleculetype ]
; Name nrexcl
LIG 1

[ atoms ]
; nr type resnr resname atom cgnr charge mass
1 SP2 1 LIG A1 1 0 54 ;
2 SN0 1 LIG A2 2 0 54 ;
3 SN0 1 LIG A3 3 0 54 ;
4 SN0 1 LIG A4 4 0 54 ;
5 SN0 1 LIG A5 5 0 54 ;
6 SN0 1 LIG A6 6 0 54 ;
7 SN0 1 LIG A7 7 0 54 ;
8 SN0 1 LIG A8 8 0 54 ;
9 SP2 1 LIG A9 9 0 54 ;

[ bonds ]
; ai aj fu c0, c1, ...
1 2 peob ;
2 3 peob ;
3 4 peob ;
4 5 peob ;
5 6 peob ;
6 7 peob ;
7 8 peob ;
8 9 peob ;

[ angles ]
; ai aj ak fu c0, c1, ...
1 2 3 peoa ;
2 3 4 peoa ;
3 4 5 peoa ;
4 5 6 peoa ;
5 6 7 peoa ;
6 7 8 peoa ;
7 8 9 peoa ;

[ dihedrals ]
; ai aj ak al fu c0, c1, ...
1 2 3 4 peod1 ;
1 2 3 4 peod3 ;
1 2 3 4 peod2 ;
1 2 3 4 peod4 ;
2 3 4 5 peod1 ;
2 3 4 5 peod3 ;
2 3 4 5 peod2 ;
2 3 4 5 peod4 ;
3 4 5 6 peod1 ;
3 4 5 6 peod3 ;
3 4 5 6 peod2 ;
3 4 5 6 peod4 ;
4 5 6 7 peod1 ;
4 5 6 7 peod3 ;
4 5 6 7 peod2 ;
4 5 6 7 peod4 ;
5 6 7 8 peod1 ;
5 6 7 8 peod3 ;
5 6 7 8 peod2 ;
```

```

5      6      7      8 peod4 ;
6      7      8      9 peod1 ;
6      7      8      9 peod3 ;
6      7      8      9 peod2 ;
6      7      8      9 peod4 ;

```

PEG3 – GROMOS 53a6_{OXY+D} (-OH terminal)

```

[ moleculetype ]
; Name          nrexcl
triethyleneglycol  3

[ atoms ]
; nr      type  resnr residue  atom  cgnr      charge      mass  typeB      chargeB
massB
; residue  1 EG3 rtp EG3  q  0.0
  1         H      1    EG3   H1    1         0.41       1.008   ; qtot 0.41
  2        OA2     1    EG3   O2    2        -0.7       15.9994 ; qtot -0.29
  3        CH2     1    EG3   C3    3         0.29       14.027   ; qtot 0
  4        CH2     1    EG3   C4    4         0.29       14.027   ; qtot 0.29
  5        OE2     1    EG3   O5    5        -0.58      15.9994 ; qtot -0.29
  6        CH2     1    EG3   C6    6         0.29       14.027   ; qtot 0
  7        CH2     1    EG3   C7    7         0.29       14.027   ; qtot 0.29
  8        OE2     1    EG3   O8    8        -0.58      15.9994 ; qtot -0.29
  9        CH2     1    EG3   C9    9         0.29       14.027   ; qtot 0
 10        CH2     1    EG3  C10   10         0.29       14.027   ; qtot 0.29
 11        OA2     1    EG3  O11   11        -0.7       15.9994 ; qtot -0.41
 12         H      1    EG3  H12   12         0.41       1.008   ; qtot 0

[ bonds ]
; ai  aj funct          c0          c1          c2          c3
  1   2   2
  2   3   2
  3   4   2
  4   5   2
  5   6   2
  6   7   2
  7   8   2
  8   9   2
  9  10   2
 10  11   2
 11  12   2

[ pairs ]
; ai  aj funct          c0          c1          c2          c3
  1   4   1
  2   5   1
  3   6   1
  4   7   1
  5   8   1
  6   9   1
  7  10   1
  8  11   1
  9  12   1

[ angles ]
; ai  aj  ak funct          c0          c1          c2          c3
  1   2   3   2
  2   3   4   2
  3   4   5   2
  4   5   6   2
  5   6   7   2
  6   7   8   2
  7   8   9   2
  8   9  10   2
  9  10  11   2
 10  11  12   2

```

[dihedrals]									
	ai	aj	ak	al	funct	c0	c1	c2	c3
c4			c5						
	1	2	3	4	1				
	2	3	4	5	1				
	3	4	5	6	1				
	4	5	6	7	1				
	5	6	7	8	1				
	6	7	8	9	1				
	7	8	9	10	1				
	8	9	10	11	1				
	9	10	11	12	1				

S.5 Discussion of Force Field Accuracy

Transfer of an alkane from oil to water can follow an indirect path with two steps: 1) transfer of an alkane from liquid alkane to gas (vaporization) and 2) transfer of an alkane from gas to liquid water (hydration). GROMOS 45a3 underwent optimization of aliphatic interaction parameters to reproduce the heat of vaporization and free enthalpy of hydration.⁶ These parameters were retained in GROMOS 53a6, so the free energy to transfer the alkane-like fatty acid tail from liquid alkane to liquid water should be accurate.⁷ The MARTINI forcefield should also be accurate; Baron et al.⁸ measured alkane/water transfer free energies for MARTINI alkanes, and their values for butane, octane, and dodecane (5.81, 9.12, 12.8 kcal/mole at 303 K) closely match the respective experimental values in Abraham et al.⁹ (5.02, 9.52, 12.85 kcal/mole at 298 K).

S.6 References for Supporting Information

- (1) Radke, C. J. Gibbs Adsorption Equation for Planar Fluid–fluid Interfaces: Invariant Formalism. *Adv. Colloid Interface Sci.*
- (2) Rowlinson, J. S.; Widom, B. *Molecular Theory of Capillarity*; Courier Corporation, 2013.
- (3) Nikas, Y. J.; Puvvada, S.; Blankschtein, D. Surface Tensions of Aqueous Nonionic Surfactant Mixtures. *Langmuir* **1992**, *8* (11), 2680–2689.
- (4) Mulqueen, M.; Blankschtein, D. Theoretical and Experimental Investigation of the Equilibrium Oil–Water Interfacial Tensions of Solutions Containing Surfactant Mixtures. *Langmuir* **2002**, *18* (2), 365–376.
- (5) Grossfield, A. *WHAM: The Weighted Histogram Analysis Method*.
- (6) Schuler, L. D.; Daura, X.; van Gunsteren, W. F. An Improved GROMOS96 Force Field for Aliphatic Hydrocarbons in the Condensed Phase. *J. Comput. Chem.* **2001**, *22* (11), 1205–1218.
- (7) Oostenbrink, C.; Villa, A.; Mark, A. E.; Van Gunsteren, W. F. A Biomolecular Force Field Based on the Free Enthalpy of Hydration and Solvation: The GROMOS Force-Field Parameter Sets 53A5 and 53A6. *J. Comput. Chem.* **2004**, *25* (13), 1656–1676.
- (8) Baron, R.; Trzesniak, D.; de Vries, A. H.; Elsener, A.; Marrink, S. J.; van Gunsteren, W. F. Comparison of Thermodynamic Properties of Coarse-Grained and Atomic-Level Simulation Models. *ChemPhysChem* **2007**, *8* (3), 452–461.
- (9) Abraham, M. H. Thermodynamics of Solution of Homologous Series of Solutes in Water. *J. Chem. Soc. Faraday Trans. 1 Phys. Chem. Condens. Phases* **1984**, *80* (1), 153–181.